HHS Public Access

Author manuscript

Ultrasound Med Biol. Author manuscript; available in PMC 2019 November 01.

Published in final edited form as:

Ultrasound Med Biol. 2018 November ; 44(11): 2323–2335. doi:10.1016/j.ultrasmedbio.2018.06.011.

Sequential payload release from acoustically-responsive scaffolds using focused ultrasound

Alexander Moncion[1,2], **Melissa Lin**[2], **Oliver D. Kripfgans**[1,2,3], **Renny T. Franceschi**[3,4,5], **Andrew J. Putnam**[3], and **Mario L. Fabiilli**[1,2,3]

[1]Applied Physics Program, University of Michigan, Ann Arbor, MI USA

[2]Department of Radiology, University of Michigan Health System, Ann Arbor, MI USA

[3]Department of Biomedical Engineering, University of Michigan, Ann Arbor, MI USA

[4]School of Dentistry, University of Michigan, Ann Arbor, MI USA

[5]Department of Biological Chemistry, University of Michigan Medical School, Ann Arbor, MI USA

Abstract

Regenerative processes, such as angiogenesis and osteogenesis, often require multiple growth factors (GFs) with distinct spatiotemporal patterns and expression sequences. Within tissue engineering, hydrogel scaffolds are commonly used for exogenous GF delivery. However, direct incorporation of GFs within conventional hydrogels does not afford spatiotemporally controlled delivery since release is governed by passive mechanisms that cannot be actively controlled after the scaffold is implanted. We have developed acoustically-responsive scaffolds (ARSs), which are fibrin scaffolds doped with payload-containing, sonosensitive emulsions. Payload release from ARSs can be controlled non-invasively and on-demand using focused, megahertz-range ultrasound. In this *in vitro* study, we develop and characterize ARSs that enable sequential release of two surrogate, fluorescent payloads using consecutive ultrasound exposures at different acoustic pressures. ARSs were generated with various combinations and volume fractions of perfluoropentane (PFP), perfluorohexane (PFH), and perfluoroheptane (PFHep) emulsions. Acoustic droplet vaporization and inertial cavitation thresholds correlated with the boiling point/molecular weight of the perfluorocarbon while payload release correlated inversely. Payload release was longitudinally measured and followed a sigmoidal trend versus acoustic pressure. PFP and PFH emulsions were stabilized when incorporated into ARSs with PFHep emulsion. These results highlight the potential of using ARSs for sequential, dual payload release for tissue regeneration.

Keywords

ultrasound; controlled release; perfluorocarbon; fibrin; acoustic droplet vaporization

Corresponding Author: Alexander Moncion, M.S, University of Michigan, 3225 Medical Sciences Building I, 1301 Catherine Street, Ann Arbor, MI 48109-5667, Phone: 305-546-6496, ambaez@umich.edu.

Introduction

Tissue regeneration is driven by the spatiotemporally-controlled expression and regulation of multiple growth factors (GFs). For example, during blood vessel growth, pro-angiogenic GFs such as vascular endothelial growth factor (VEGF) and fibroblast growth factor (FGF) stimulate endothelial cell migration, mitogenesis, and sprouting (Abe, et al. 2013, Akeson, et al. 2003, Cao, et al. 2003, Li, et al. 2010, Ruhrberg, et al. 2002, Saik, et al. 2011). The newly sprouting vessels are then stabilized by pericytes, which are recruited by platelet derived growth factor (PDGF). During the healing of a bone fracture, bone morphogenetic protein 2 (BMP2) initially stimulates callus formation during the inflammation stage. Later, VEGF causes vascular in-growth from the periosteum. Reviews more fully highlight the complex, temporal orchestration of GF signaling involved in the multiple stages of angiogenesis and osteogenesis (Ai-Aql, et al. 2008, Carmeliet and Jain 2011).

Hydrogel scaffold-based delivery systems can provide sequential delivery of multiple GFs to enhance tissue regeneration. The motivation for generating these scaffolds is that sequential delivery of GFs can mimic critical aspects of endogenous GF signaling more closely. Additionally, certain GFs (e.g., bFGF and PDGF) are mutually antagonistic when present simultaneously (Tengood, et al. 2011), thus further highlighting the need for sequential delivery. Sequential delivery of two GFs (e.g., GF1, GF2) has been obtained by designing a composite scaffold using one of two general strategies. First, GF1 is incorporated into a scaffold while GF2 is pre-encapsulated into particles which are then incorporated into the scaffold (Richardson, et al. 2001). This therapeutic approach typically results in GF1 being released at a faster rate than GF2. Second, GF1 and GF2 are pre-encapsulated into separate particles, which are then incorporated into a scaffold (Basmanav, et al. 2008). In both strategies, the release kinetics of the GFs are dependent on the material properties of both the scaffold and particles such as crosslinking density, pore size, GF affinity, and charge. Sequential delivery of VEGF/PDGF (Awada, et al. 2015), bFGF/BMP-2 (Lee and Koh 2014), BMP-2/BMP-7 (Basmanav, et al. 2008), VEGF/BMP-2 (Kempen, et al. 2009), and BMP-2/insulin-like growth factor (IGF-1) (Kim, et al. 2012) has been demonstrated using the previously mentioned techniques.

A critical limitation of the previous sequential delivery strategies is that the release kinetics of GF1 and GF2 are designed *a priori*. Therefore, after the scaffold is implanted at, or adjacent to, the site of intended tissue regeneration the release kinetics – including the initial timing of release of GF1 and GF2 – cannot be altered. From a clinical perspective, this is potentially problematic since the release kinetics of the multiple encapsulated GFs cannot be adjusted based on the actual progress of tissue regeneration within a patient. Thus, scaffold-based delivery systems that enable active modulation of sequential release would be beneficial.

We have developed a scaffold-based delivery system where release of a bioactive payload is controlled non-invasively and in an on-demand manner using focused, megahertz-range ultrasound (US). These acoustically-responsive scaffolds (ARSs) consist of a fibrin hydrogel doped with a micron-sized, perfluorocarbon (PFC) double emulsion (Moncion, et al. 2016, Moncion, et al. 2017). Fibrin was chosen as the hydrogel due to its biocompatibility, ability

to degrade with minimal inflammatory response, potential for autologous sourcing, and low viscoelastic properties that help facilitate cell migration (Lee and Mooney 2001, Markert, et al. 2013). A water-soluble payload is encapsulated within the PFC double emulsion having a water-in-PFC-in-water (W_1/PFC/W_2) structure. When exposed to pulsed (i.e., non-thermal) US above a certain pressure, the PFC phase within the emulsion vaporizes in a process known as acoustic droplet vaporization (ADV), which causes release of the encapsulated payload (Fabiilli, et al. 2009, Kripfgans, et al. 2000, Moncion, et al. 2016).

We demonstrated that release of a single payload from an ARS is a threshold based phenomenon, which is dependent on properties of the emulsion and the fibrin scaffold (Moncion, et al. 2016). Recently, we have shown, both *in vitro* and *in vivo,* that US can modulate the release of bFGF from an ARS, with a potential application in therapeutic angiogenesis (Moncion, et al. 2017). In the current *in vitro* study, we demonstrate for the first time that US can control the sequential release of two surrogate payloads, Alexa Fluor 488-labelled dextran and Alexa Fluor 594-labelled dextran, from an ARS. These payloads were chosen for this proof-of-concept study since they can be spectrally differentiated. To achieve sequential release, we formulate ARSs containing two separate emulsion populations, each containing a different PFC (Figure 1A). This strategy was inspired by previous publications demonstrating the inverse relationship between the minimum acoustic pressure required for ADV (i.e., the ADV threshold) and the boiling point of the dispersed PFC phase within the emulsion (Fabiilli, et al. 2009, Kawabata, et al. 2005, Sheeran, et al. 2011).

Materials and Methods

Preparation and Characterization of the Double Emulsion

Double emulsions with a water-in-PFC-in-water (W_1/PFC/W_2) structure were prepared using a previous method (Moncion, et al. 2017). Briefly, a triblock fluorosurfactant, consisting of Krytox 157FSH (CAS# 51798-33-5, DuPont, Wilmington, DE, USA) and polyethylene glycol (MW: 1000, CAS#: 24991-53-5, Alfa Aesar, Ward Hill, MA USA), was dissolved at 2% (w/w) in 1 g of perfluoropentane (PFP, CAS# 678-26-2, Strem Chemicals, Newburyport, MA USA), perfluorohexane (PFH, CAS# 355-42-0, Strem Chemicals), or perfluoroheptane (PFHep, CAS#: 335-57-9, Sigma-Aldrich, St. Louis, MO USA). For PFP and PFH emulsions, the PFC solution was combined at 2:1 (v/v) with a W_1 phase containing 1.66 mg/mL Alexa Fluor 488-labeled dextran (AF488, MW: 10,000 Da, Life Technologies, Grand Island, NY USA) in phosphate-buffered saline (PBS, Life Technologies). For PFHep emulsions, the PFC solution was combined with a 3.32 mg/mL solution of Alexa Fluor 594-labeled dextran (AF594, MW: 10,000 Da, Life Technologies) in PBS. The PFC and W_1 phases were emulsified using a probe sonicator (Q55, QSonica, Newton, CT USA) for 30 seconds while on ice. The resulting primary emulsion, with a water-in-PFC (W_1/PFC) structure, was pumped at 0.5 μL/min through an in-line filter (0.5 μm stainless steel frit, Cat#: 24993, Restek, Bellefonte, PA, USA) and then into the inner channel of a quartz microfluidic chip (Cat#: 3200146, junction: 14 × 17 μm, hydrophilic coating, Dolomite, Royston, United Kingdom) using a syringe pump (KDS-410, kd Scientific, Holliston, MA USA). Simultaneously, 50 mg/mL Pluronic F68 (CAS# 9003-11-6, Sigma-Aldrich) in PBS

was pumped at 2.5 μL/min though an in-line filter and then into the outer channels of the chip using a second syringe pump (78-0388, kd Scientific). The chip was mounted on an inverted microscope (DMIL, Leica Microsystems, Buffalo Grove, IL USA) which enabled visualization of emulsion production. Emulsion was collected following equilibration of the chip and then stored at 5°C until use.

Emulsions were characterized with a Coulter Counter (Multisizer 4, Beckman Coulter, Brea, CA USA) in the range of 1-30 μm. To confirm emulsion morphology, the emulsion was imaged using an inverted confocal microscope (SP5X, Leica Microsystems, Inc., Buffalo Grove, IL USA) at the University of Michigan Microscopy & Image Analysis Laboratory. One day after production of the emulsion, the concentration of dextran in the W_2 phase was measured with a plate reader (Molecular Devices, SpextraMax M2e, Sunnyvale, CA USA). The encapsulation efficiency of dextran in the emulsion was calculated via a mass balance. Using the PFP and PFH emulsions, we determined that this technique was equivalent to our previous method of measuring encapsulation efficiency via breaking the emulsion pellet (Moncion, et al. 2016).

Fabrication of ARSs for Acoustic Characterization

ARSs were prepared using 10 mg/mL clottable protein by first combining bovine fibrinogen (Sigma-Aldrich) dissolved in degassed (36% O_2 saturation) FluoroBrite Dulbecco's modified Eagle's medium (DMEM, Life Technologies), with 10% (v/v) bovine thrombin (20 U/mL, Thrombin-JMI, King Pharmaceuticals, Bristol, TN, USA), 0.025 U/mL aprotinin (Sigma-Aldrich), and 1.0% (v/v) of PFP, PFH, or PFHep emulsion. The ADV and inertial cavitation (IC) thresholds of the ARSs were determined using previously described methods (Moncion, et al. 2016). Briefly, 0.5 mL ARSs (height: 0.28 cm) were cast in 24-well Bioflex plates (Flexcell International, Burlington, NC, USA) by aliquoting the ARS mixture into each well and allowing it to polymerize for 30 min at room temperature. The ARSs were exposed to focused US generated by a calibrated, single-element transducer (2.5 MHz, H108, f-number = 0.83, focal length = 50 mm, Sonic Concepts, Inc., Bothell, WA USA) in the range of 0 to 8.0 MPa peak rarefactional pressure. The bottom of each well in the plate consisted of a silicone elastomer membrane, which based on a thickness of 1 mm, attenuated the US by less than 2% (Garvin, et al. 2010). The complete acoustic setup is described above. A calibrated hydrophone (HGL-0085, dynamic range = 1-50 MHz, Onda, Sunnyvale, CA USA) was placed 6 cm away from the focus of the transducer to detect backscattered acoustic signals generated in the ARS during the US exposure. The radiofrequency signals collected with the hydrophone and digitized by an oscilloscope (sampling rate = 100 MHz) were analyzed in MATLAB (The MathWorks, Natick, MA, USA). The ADV threshold was determined by analyzing the fundamental frequency (2.5 MHz) since bubbles formed in the ARS due to ADV significantly increase the scattered, fundamental signal (Reznik, et al. 2011, Schad and Hynynen 2010). The ADV threshold was defined as the lowest acoustic pressure at which the statistical increase in fundamental signal over background was observed. The IC threshold was computed using the broadband signal from the acquired radiofrequency waveforms using identical methods as described previously (Moncion, et al. 2016).

US Exposure

All acoustic exposures were conducted using the following setup (Moncion, et al. 2016). The single-element transducer was driven by pulsed waveforms generated using a dual channel function generator (33500B, Agilent Technologies, Santa Clara, CA USA), amplified by a gated radiofrequency amplifier (GA-2500A Ritec Inc, Warwick, RI USA), and passed through a matching circuit (H108_3MN, Sonic Concepts) for radiofrequency impedance matching between the transducer and amplifier. Gating of the carrier waveform was realized using the second channel of the function generator, resulting in a pulsed signal. All generated and amplified signals were monitored with an oscilloscope (HDO4034, Teledyne LeCroy, Chestnut Ridge, NY USA). All acoustic exposures were done with the following parameters unless otherwise stated: 2.5 MHz fundamental frequency, 0.8 to 8.0 MPa peak rarefactional pressure, 13 acoustic cycles, and 100 Hz pulse repetition frequency (PRF). All US pressures are listed as peak rarefactional pressures.

To localize the axial focus of the US transducer with respect to the ARS, a pulse echo technique was used. Briefly, the single element transducer was driven by a pulser-receiver (5077PR, Olympus, Center Valley, PA US) that generated a low energy signal at 100 Hz PRF. The reflected signal was visualized on an oscilloscope, and maximized in amplitude by modifying the distance between the transducer and ARS. Using this technique, the axial focus of the transducer was positioned at mid-height of the ARS.

Single Payload Release

The goal of this experiment was to characterize single payload release as a function of acoustic pressure. As seen in Table 1, four ARSs compositions were interrogated for the single payload release studies. ARSs were fabricated with either 0.33 or 0.67% (v/v) emulsion in a modified 48-well plate (Thermo Fisher Scientific, Waltham, MA, USA) in which the plate bottom was drilled out and replaced with a Tegaderm film (3M Health Care, St. Paul, MN, USA). The ARSs, 0.3 mL volume per well (height: 0.32 cm), were allowed to polymerize for 30 min at room temperature. Each ARS was then covered with 0.3 mL of overlying media, consisting of FluoroBrite DMEM supplemented with 100 U/mL penicillin and 100 μg/mL streptomycin. The ARSs were placed in a standard tissue culture incubator (37°C, 5% carbon dioxide), except during the US exposure.

One day after polymerization, the plate containing the ARSs was placed in a tank of degassed water (30-36% O_2 saturation) at 37°C such that only the bottom half of the plate was submerged. Using pulse-echo, the single element US transducer was positioned under the plate such that the axial focus was located at mid-height of the ARS. During US exposure, the transducer was manually rastered, using a 2-axis translational stage, across the entire ARS until the entire surface area was exposed to US. The overlying media was sampled daily for three days by collecting half of the media and replacing the sampled volume with an equal volume of fresh media. On the day of US exposure, the media was sampled immediately after exposure. The concentration of dextran released into the sampled media was measured using a plate reader (Molecular Devices). As a comparison, the release of unencapsulated dextran, incorporated directly into the fibrin scaffold, was also measured.

Dual Payload Release

Figure 1A schematically shows the strategy used to obtain sequential dual payload release from ARSs. As seen in Table 1, two different ARSs compositions, PFP/PFHep-ARSs or PFH/PFHep-ARSs, were interrogated for the dual payload release studies. The acoustic pressures used for exposure were selected based on results obtained from the acoustic characterization and single payload release studies. Two different exposure schemes were used. For single US exposure, PFP/PFHep-ARSs were exposed to US at 2 or 8 MPa one day after polymerization, while PFH/PFHep-ARSs were exposed to US at 2.6 or 8 MPa one day after polymerization. For sequential US exposures, PFP/PFHep-ARSs were exposed to US at 2 and 8 MPa one day and three days after polymerization, respectively. Similarly, PFH/PFHep-ARSs were exposed to US at 2.6 and 8 MPa one and three days after polymerization, respectively. Similar to the single payload experiments, the overlying media was sampled daily for three days by collecting half of the media and replacing the sampled volume with an equal volume of fresh media. For the initial US exposure, the media was sampled immediately after US exposure. For samples that had US exposure on day three, the media was sampled immediately before and after US exposure. The concentration of each dextran in the sampled media was measured using a plate reader.

Statistics

All statistical analyses were performed using GraphPad Prism software (GraphPad Software, Inc., La Jolla, CA USA). All data is expressed as the mean plus/minus the standard deviation of measured quantities. In some cases, the error bars are smaller than the symbol representing the data points. All *n*-values are listed below each corresponding figure. Payload release data, collected as a function of acoustic pressure, was fit to a 4-parameter sigmoid function where the following parameters are reported: maximum payload release (R_{max}), minimum payload release (R_{min}), and the acoustic pressure at which half of maximum payload release was observed (P_{50}). The 95% confidence intervals of R_{max}, R_{min}, and P_{50} are listed in the format S [S_L, S_H], where S is the average value, S_L is the lower bound value, and S_H is the upper bound value. Statistically significant differences of all data sets were determined with a Student's *t*-test corrected for multiple comparisons using the Holm-Sidak method, with differences deemed significant for $p<0.05$.

Results

Emulsion and ARS properties

Table 2 displays the characteristics of the double emulsions used in the ARSs. No statistically significant differences in the encapsulation efficiency, mean diameter, and droplet concentration were observed between any of the emulsion formulations. The PFP emulsion had a greater coefficient of variance than either the PFH or PFHep emulsion. The ADV thresholds of ARSs with PFH emulsion (i.e., PFH-ARSs) or PFHep emulsion (PFHep-ARSs) was lower than their respective IC thresholds. Additionally, ARSs with PFP emulsion (i.e., PFP-ARSs) had a significantly lower ADV threshold than PFH- and PFHep-ARSs, while no differences were observed between the ADV thresholds of PFH- and PFHep-ARSs. The IC threshold of PFHep-ARSs was higher than the IC threshold in PFP-ARSs. Confocal microscopy images of a dual payload containing ARS in shown in Figure 1B. The two

emulsions, containing AF488 (green) or AF594 (red) in the W_1 phase, were dispersed within the fibrin scaffold containing Alexa Fluor 647-labeled fibrinogen (magenta). The double emulsion droplets appeared uniform in size and the W_1 droplets were submicron in diameter.

Dextran release from a conventional fibrin scaffold

Release of the unencapsulated dextrans, which were incorporated directly into a conventional fibrin matrix, is shown in Figure 2. There was significant release of both dextrans one day after the scaffold was formulated, resulting in 44.01 ± 1.00% and 40.13 ± 0.62% release of AF488 and AF594, respectively. On day 7 there was 73.98 ± 1.61% and 71.34 ± 1.21% release of AF488 and AF594, respectively, with statistically significant differences between the two conditions occurring on days 1-5.

Pressure dependent dextran release from single payload-containing ARSs

Figure 3(A-D) shows the release of a single payload from different ARS formulations as function of acoustic pressure and time. The release from PFH- and PFHep-ARSs had a sigmoidal profile on days 2 and 3, with more release observed at acoustic pressures above, and near, the ADV threshold while being asymptotic at the highest pressures interrogated in this work. On day 1, there were no differences in payload release across the range of acoustic pressures. In addition, all ARS formulations yielded more payload release on day 3 compared to days 1 and 2. PFP-ARSs had the most payload release in the absence of US (i.e., 0 MPa), with 8.75 ± 0.77% released on day 3, compared to 1.54 ± 0.22, 0.78 ± 0.11, and 1.65 ± 0.23% payload release for ARSs with 0.67% (v/v) PFH, 0.67% (v/v) PFHep, and 0.33% (v/v) PFHep emulsions, respectively, at the same time point. The most payload release was observed from ARSs with 0.33% (v/v) PFHep emulsion, with 18.07 ± 2.25% release at 8 MPa. Conversely, ARSs with 0.33% (v/v) PFP, 0.67% (v/v) PFH, 0.67% (v/v) PFHep emulsions had 15.35 ± 0.93, 10.66 ± 0.41, and 5.30 ± 0.88% released, respectively, at the same pressure and time point.

Pressure dependent dextran release from dual payload-containing ARSs

Release of two payloads from an ARS following a single US exposure is shown in Figure 4(A-D). Similar to single emulsion-containing ARSs, all dual payload ARS conditions displayed a sigmoidal release profile on days 2 and 3. Similar to PFP-ARSs, the most payload release in the absence of US was observed from the PFP emulsion within PFP/PFHep-ARSs (Figure 4A), resulting in statistically different releases of 1.46 ± 0.21%, 5.21 ± 0.58%, and 7.73 ± 0.54% on days 1, 2, and 3, respectively. Contrastingly, within the same PFP/PFHep-ARS, the PFHep emulsions had 0.70 ± 0.21%, 1.07 ± 0.31%, and 1.45 ± 0.37% payload release on days 1, 2, and 3 in the absence of US. The highest overall release among the conditions tested was observed from the PFH emulsion within the PFH/PFHep-ARS; on day 3, 9.82 ± 0.65% release was observed following exposure to 8 MPa. The lowest release, 3.14 ± 0.39%, measured on day 3 following exposure to 8 MPa US was from the PFHep emulsion in the PFH/PFHep-ARS (Figure 4D). With PFP/PFHep-ARSs (Figure 4A-B), US exposure at 8 MPa yielded greater release on day 3 from the PFP emulsion (7.73 ± 0.54%) versus the PFHep emulsion (6.72 ± 0.45%). For PFH/PFHep-ARSs (Figure 4C-D), US exposure at 8 MPa generated greater release on day 3 from the PFH emulsion (9.82 ± 0.65%) versus the PFHep emulsion (3.14 ± 0.39%).

Dual payload release from single and multiple ultrasound exposures

Figure 5A and 5B display the release profiles of PFP/PFHep-ARSs and PFH/PFHep-ARSs, respectively, following a single US exposure on day 1. PFP/PFHep-ARSs were exposed to either 2 or 8 MPa whereas PFH/PFHep-ARSs were exposed to 2.6 or 8 MPa. Figure 5A highlights that exposure at 8 MPa generated more payload release than 2 MPa from both PFP (10.20 ± 0.46% vs. 5.53 ± 0.86%) and PFHep (6.87 ± 0.86% vs. 2.47 ± 0.33%) emulsions by day 7. US exposure at 8 MPa yielded significantly greater release than 2 MPa on days 1-7 for PFP emulsion and days 2-7 for PFHep emulsion. The same trend was observed with PFH/PFHep-ARSs (Figure 5B), with more payload release at 8 MPa than at 2.6 MPa by day 7 for PFH (17.80 ± 2.29% vs. 9.22 ± 0.44%) and PFHep (3.71 ± 0.45% vs. 2.37 ± 0.17%) emulsions. US exposure at 8 MPa generated significantly greater release than 2.6 MPa on days 2-6 for PFH emulsion and days 3-7 for PFHep emulsion.

Figure 5C shows the release profiles of PFP/PFHep-ARSs following sequential US exposures on day 1 and day 3 of 2 MPa and 8 MPa, respectively. By day 7, PFP/PFHep-ARSs exposed to US (i.e., labeled as '+US') had greater release than controls not exposed to US (i.e., labeled as '-US'), with 8.84 ± 0.45% vs. 4.66 ± 0.55% released from PFP and 9.39 ± 2.73% vs. 1.40 ± 0.04% for PFHep emulsions. Statistically significant differences were observed on days 1-7 for both emulsions. The release from PFP emulsion on day 3 (prior to the second US exposure at 8 MPa) was 3.06 ± 0.16%, which is not statistically different and consistent with the release observed in Figure 5A (i.e., 3.09 ± 0.53% released by day 3 at 2 MPa). A similar trend was observed from PFHep emulsions (Figure 5C), with 1.62 ± 0.33% released by day 3 (prior to the second US exposure at 8 MPa). This is also not statistically different and consistent with the release observed in Figure 5A (i.e., 1.31 ± 0.20% released by day 3 at 2 MPa). For PFP emulsion, the second US exposure at 8 MPa on day 3 yielded greater release by day 7 (8.84 ± 0.45%) compared to release observed at day 7 following a single US exposure of 2 MPa on day 1 (5.53 ± 0.86%). Analogously for PFHep emulsion, exposure to 8 MPa US on day 3 generated greater release by day 7 compared to release obtained on day 7 following a single US exposure of 2 MPa on day 1 (9.39 ± 2.73% vs. 2.47 ± 0.33%).

Figure 5D shows the release profiles of PFH/PFHep-ARSs following sequential US exposures on day 1 and day 3 of 2.6 MPa and 8 MPa, respectively. The observed trends are similar to those of PFP/PFHep-ARSs (Figure 5C), with more release on day 7 in the +US case (PFH: 11.12 ± 0.86%; PFHep: 3.79 ± 0.57%) compared to their respective −US condition (PFH: 2.46 ± 0.49%; PFHep: 1.73 ± 0.69%). For PFH emulsion, the second US exposure at 8 MPa on day 3 yielded a statistically greater release by day 7 (11.12 ± 0.86%) compared to the release observed at day 7 following a single US exposure of 2.6 MPa on day 1 (9.22 ± 0.44%). Analogously for PFHep emulsion, exposure to 8 MPa US on day 3 generated greater release by day 7 compared to release obtained on day 7 following a single US exposure of 2 MPa on day 1 (3.79 ± 0.57% vs. 2.37 ± 0.17%). Overall, 4.5- and 2.2-fold increases in release were observed for the +US conditions from the PFH and PFHep emulsions, respectively, in the PFH/PFHep construct, compared to their respective −US conditions in Figure 5D on day 7.

Stability of single and dual payload-containing ARSs

The macroscopic appearances of the various ARS formulations, for +US and −US conditions, are displayed in Figure 6. For the +US condition, day 1 images were taken immediately after US exposure. ARSs without bubbles appear relatively featureless, as was the case for the -US condition with 0.66% (v/v) PFHep emulsion. Comparatively, as the emulsion within the ARS vaporized, gas bubbles became evident, as clearly seen with PFP-ARSs. For the −US condition, there was qualitatively the most bubble formation in PFP-ARSs, followed by PFH-ARSs, PFH/PFHep-ARSs, and PFP/PFHep-ARSs. Qualitatively, the number and/or size of the bubbles increased from day 1 to day 2 for all of the ARS formulations, except for PFHep-ARS. There were more bubbles in the ARSs on day 1 and day 2 for the +US condition versus the matching −US condition. For PFP-ARSs or PFH-ARSs, the bubble density observed on day 2 for the +US condition was very high, with bubbles encompassing the entire volume of the ARS. For both +US and −US conditions, there was little to no bubble formation in either ARS formulation containing PFHep emulsion.

Discussion

In this work, sequential release of two payloads from an ARS was demonstrated by encapsulating each payload within separate sonosensitive emulsions having unique ADV thresholds. The ability to release multiple payloads from one ARS can ultimately increase the understanding of how various temporal profiles and sequences of GFs impact tissue regeneration. Overall, the highly versatile nature of ARSs, including the ability to modulate matrix (e.g., scaffold density), emulsion (e.g., droplet size) (Moncion, et al. 2016, Moncion, et al. 2016), and US (e.g., acoustic pressure) properties provides a highly tunable approach for delivering multiple payloads in tissue engineering applications.

A critical component of ARSs is the sonosensitive emulsion containing each payload. Our work has demonstrated that monodispersed emulsions have superior stability compared to their polydispersed counterparts, and can be used for bioactive growth factor delivery (Moncion, et al. 2017). In the current study, the ADV thresholds correlated with the boiling point and molecular weight of the dispersed PFC phase for similarly-sized, monodispersed emulsions. It has been hypothesized that the effective boiling point of the PFC within the emulsion is one of the factors determining the ADV threshold (Moncion, et al. 2016, Rapoport, et al. 2011, Reznik, et al. 2013), with smaller droplets experiencing a higher boiling point elevation due to the Laplace pressure gained from droplet formation (Rapoport, et al. 2009, Sheeran, et al. 2011). Thus, emulsions made from low-boiling point PFCs such as PFP and perfluorobutane are stable at body temperature when formulated as submicron droplets. An alternative hypothesis is that the ADV threshold is dependent on the energy barrier for homogeneous nucleation within the PFC liquid, with the energy required to create a vapor embryo correlating with the molecular weight of the PFC (Miles, et al. 2016, Mountford and Borden 2016). Furthermore, others have shown that the droplet-to-bubble transition is dependent on the dissolved oxygen content within the PFC (Rapoport, et al. 2011), with oxygen solubility inversely proportional to the PFC molecular weight (Riess 2001).

Emulsions have been formulated using ad-mixtures of two different PFCs (Barnabe-Heider, et al. 2005, Kawabata, et al. 2005, Moncion, et al. 2016). For an emulsion containing an ad-mixture of low boiling point PFCs (e.g., perfluoropropane and perfluorobutane), the vaporization threshold was close to an emulsion made solely of the higher boiling point PFC (i.e., perfluorobutane) (Sheeran, et al. 2012). It was determined that in an open system the lower boiling (i.e., smaller molecular weight) PFC preferentially dissolved, thereby enhancing the fraction of higher boiling point PFC within each droplet (Mountford, et al. 2015).This effect was not observed in our previous publication where the ADV threshold of an ARS containing emulsion with a 1:1 ad-mixture of PFP:PFH was intermediate to that of PFP and PFH (Moncion, et al. 2016). In this study, each emulsion was formulated with only one PFC. However, when formulating an ARS with two different emulsions, it is possible that counterdiffusion of PFCs could occur, which may explain some of the observed differences between single and dual payload-containing ARSs.

The ADV thresholds, measured in ARSs with a single emulsion type, can be used in selecting which two emulsion formulations can be combined into a single ARS for dual payload release. For example, PFP- and PFHep-ARSs have statistically different ADV thresholds. Thus, an interval of acoustic pressures exists that will vaporize the PFP emulsion while minimally affecting the PFHep emulsion. Interestingly, this is not the case with PFH- and PFHep-ARSs, which do not have statistically different ADV thresholds. However, there was a difference when PFH and PFHep emulsions are combined in a single ARS, as seen with the release profiles for PFH-ARS (Figure 3C) versus PFH emulsion in a PFH/PFHep-ARS (Figure 4C). The P_{50} (Supplemental Table 1 and 2) was 1.70 MPa [1.54, 1.87] and 3.12 MPa [2.84, 3.46] for PFH release from PFH-ARSs and PFH/PFHep-ARSs on day 3, respectively. A similar trend was also observed with PFHep-ARSs and PFHep emulsion in PFH/PFHep-ARSs, where the P_{50} was 3.23 MPa [2.99, 3.54] and 3.98 MPa [3.50, 4.73] for PFHep release from PFH-ARSs and PFH/PFHep-ARSs on day 3, respectively. However, payload release in the absence of US (indicated by the R_{min} values in Supplemental Tables 1 and 2) remained unchanged, with 1.33% [0.66, 1.99] and 1.18% [0.56, 1.75] release from PFH-ARSs and PFH emulsions in PFH/PFHep-ARSs on day 3, respectively, and 1.38% [0.70, 2.01] and 0.60% [0.28, 0.88] release from PFHep-ARSs and PFHep emulsion in PFH/PFHep-ARSs at the same time point. However, in the absence of US, there was a significant difference when comparing PFP release from PFP-ARSs and PFP/PFHep-ARSs, with 8.75 ± 0.77% versus 3.61 ± 0.29% released by day 3, respectively. Thus, the amount of spontaneous release from the lower boiling point emulsion decreased when combined in an ARS with a higher boiling point emulsion. This is also qualitatively supported by Figure 6, where PFP/PFHep-ARSs contain less bubbles than PFP-ARSs and PFH/PFHep-ARSs contain less bubbles than PFH-ARSs for the −US condition. The sigmoidal fit did not converge for the release from PFP-ARSs and PFP emulsions in a PFP/PFHep-ARS construct.

Similar to our previous studies using a single emulsion type (Moncion, et al. 2016, Moncion, et al. 2016, Moncion, et al. 2017), the sum total of both emulsions in the dual payload ARSs was 1% (v/v). Another interesting trend was observed for the maximum payload release (indicated by R_{max} in Supplemental Tables 1 and 2). For example, values of R_{max} for PFHep-ARSs on day 3 were 4.94% [4.69, 5.27] and 17.15% [16.08, 18.66] for single

payload ARSs containing 0.67% (v/v) and 0.33% (v/v) PFHep emulsion, respectively. R_{max} values for PFHep emulsion in a dual payload ARS were 7.12% [6.38, 8.66] and 3.19% [2.85, 3.98] for emulsion loadings of 0.67% (v/v) and 0.33% (v/v), respectively. Thus, for the higher volume fraction (i.e., 0.67% (v/v)) of PFHep emulsion, there was an increase in payload release when combined with PFP emulsion in the PFP/PFHep-ARS. Conversely, for the lower volume fraction (i.e., 0.33% (v/v)) of PFHep emulsion, there was a significant decrease in R_{max} when comparing single versus dual payload ARSs. It is hypothesized that acoustic shadowing caused by the vaporization of the PFH emulsion, which was present at a 2:1 (v/v) ratio, caused the reduction in payload release from the PFHep emulsion in the PFH/PFHep-ARS. There is likely a volume fraction for the emulsion-containing payload 1 below which acoustic shadowing will not be an issue for the emulsion containing payload 2. However, for therapeutic applications, this volume fraction must be balanced with respect to delivering an adequate amount of GF that can elucidate a biological response. In our previous publication, US-triggered delivery of 1 μg of bFGF from an ARS containing 1% (v/v) PFH emulsion yielded significant angiogenesis in mice with subcutaneously-implanted ARSs (Moncion, et al. 2017). Other studies in mice have demonstrated stimulation of angiogenesis with subcutaneously-implanted hydrogels containing 0.2-100 μg bFGF (Cai, et al. 2005, Tabata, et al. 1999). In the critical limb ischemia model, bFGF doses ranging from 40 ng to 25 μg, in combination with granulocyte colony stimulating factor, induced angiogenesis in mice (Jeon, et al. 2006, Layman, et al. 2012). This wide range of reported bFGF doses highlights the lack of consensus regarding the therapeutically effective dose of bFGF required for in vivo studies. Comparatively, 30 ng/mL bFGF can stimulate angiogenic sprouting in vitro models of vascular morphogenesis (Nehls, et al. 1998).

Sequential payload release from an ARS is dependent on sequential US exposures. A potential limitation of this approach is the generation of bubbles following the first US exposure that can remained entrapped within the scaffold, as seen in histological images from our previous publication (Moncion, et al. 2016), thus attenuating (e.g., shadowing) subsequent US exposures. However, when the ARS is implanted *in vivo*, the biodegradability of the fibrin matrix provides a means by which the host can remove the entrapped gas bubbles, or remodel the implant altogether (Ceccarelli and Putnam 2014). This could reduce the extent to which bubbles affect subsequent US exposures. Additionally, as the US pressure increases, the volume of the US focus that is above the ADV threshold increases, thereby enabling the vaporization of droplets that were not previously vaporized and may be located between bubbles. This mechanism is potentially observed in Figures 5C and 5D, where the rate of payload release from the emulsion with the lower ADV threshold (i.e., PFP in PFP/PFHep-ARSs and PFH in PFH/PFHep-ARSs) increased after the second US exposure. Thus, the second US exposure either vaporized additional droplets or increased the rate of diffusion of dextran that was released from the first US exposure (Moncion, et al. 2016).

Most importantly, for PFH/PFHep-ARSs the release from the PFHep emulsion was not different from the −US control prior to the second US exposure (Figure 5D). Thus, PFH/PFHep-ARS provide a more controlled dual payload release compared to PFP/PFHep-ARSs, of which the release from PFHep emulsions was not different prior to the second US exposure at 8 MPa. This lack of statistical difference, even with a lower initial US pressure

exposure of the PFP/PFHep-ARSs (2 MPa) than with PFH/PFHep-ARSs (2.6 MPa), could be due to the instability of the entire ARS construct caused by the PFP emulsion.

High payload retention in the absence of US is crucial for controlled release from an ARS. Figure 2 shows that a significant amount of burst release occurs when the dextrans are incorporated directly into a conventional fibrin scaffold (i.e., without any emulsion), with 44.01 ± 1.00% and 40.13 ± 0.62% released for AF488 and AF594 dextrans, respectively, by day 1 Even the ARS formulation with the greatest non-selective release (i.e. PFP-ARS, Figure 3A) displayed better payload retention than the non-emulsified dextrans. The higher amount of release from AF488 dextran versus AF594 dextran was likely due to the higher molecular weight of the latter dextran.

When developing a scaffold-based release technology, there are critical differences that should be considered when using dextran as a surrogate payload for a GF. Though the utilized dextrans (10 kDa) have molecular weights on the same order as bFGF (16 kDa) or BMP-2 (26 kDa), these GFs as well as others can bind to fibrin(ogen) via its heparin-binding domains (Martino, et al. 2013, Sahni, et al. 1998). This binding can reduce the amount of burst release observed with GFs from fibrin-based scaffolds (Jeon, et al. 2005). The retention of a GF within fibrin could be used as an alternative approach for the sequential delivery of two GFs from an ARS. For example, one GF could be encapsulated within the emulsion and released by US; another GF could be incorporated directly into the scaffold, with release kinetics controlled by scaffold binding and degradation. Furthermore, successful GF delivery requires the release of a GF that is bioactive, which is dependent on higher level protein structures that can be affected by elevated US pressures (Marchioni, et al. 2009). Since pulsed US has been used to trigger release from ARSs, mechanical (e.g., cavitation) effects could impact the bioactivity of released GF. However, our prior work demonstrated that 8 MPa (peak rarefactional) US at 2.5 MHz can be used to release bioactive bFGF both in vitro and in vivo (Fabiilli, et al. 2013, Moncion, et al. 2017).

Two parameters that were not explored in this study but warrant future investigation are droplet diameter and ultrasound frequency. Previous studies have shown that the ADV threshold correlates inversely with droplet diameter (Fabiilli, et al. 2009, Schad and Hynynen 2010, Sheeran, et al. 2011) and ultrasound frequency (Kripfgans, et al. 2000). Thus, it is possible to further optimize dual payload release from an ARS by using different droplet sizes and/or different ultrasound frequencies to trigger ADV in each droplet population. Additionally, each emulsion could be incorporated anisotropically within the ARS. For example, a bilayer ARS could be generated with each layer containing a different emulsion with a unique ADV threshold and payload. The layers proximal and distal from the US transducer would contain emulsions with higher and lower thresholds, respectively. This bilayer configuration would reduce the effects of acoustic shadowing. A limitation of this bilayer approach is the difficulty in achieving in situ polymerization of the ARS for in vivo applications, though pre-polymerized scaffolds could be implanted within subcutaneous or intramuscular pockets created via surgical incision.

Conclusion

We have demonstrated that focused, 2.5 MHz US can sequentially release two fluorescent payloads, each encapsulated within a separate monodispersed PFC double emulsion, that are contained within a single ARS. The release strategy involved sequential US exposures, whereby the first and second payloads were released at lower and higher acoustic pressures, respectively. ADV and IC thresholds correlated with the boiling point/molecular weight of the PFC within the emulsion. Payload release in the absence and presence of ultrasound was inversely correlated with the boiling point/molecular weight of the PFC. In general, payload release from the ARSs displayed a sigmoidal trend as a function of acoustic pressure, with increasing release over time in response to a single US exposure. Overall, PFH/PFHep-ARSs showed more controlled release when exposed to US, with release of the first payload from the PFH emulsion occurring after the initial US exposure and the release of the second payload from PFHep emulsion occurring after the second US exposure. The stability of PFP and PFH emulsions increased when combined with PFHep emulsion in one ARS. These results show that ARSs, in conjunction with focused US, have the potential of delivering two therapeutic payloads (e.g., GFs) in a temporally controlled manner. Future work will focus on optimizing the amount of selective release from the dual payload ARS, as well as demonstrating the release of two bioactive GFs for tissue regeneration.

Supplementary Material

Refer to Web version on PubMed Central for supplementary material.

Acknowledgements

This work was supported in by NIH grant R01HL139656 (MLF) and the Basic Radiological Sciences Innovative Research Award (MLF). AM was supported by the National Science Foundation Graduate Student Research Fellowship (Grant No. DGE 1256260). ML was supported by funds from the Undergraduate Research Opportunity Program. Special thanks to Dr. Allen F. Brooks for aiding in the synthesis of the fluorosurfactant used to formulate the double emulsions.

REFERENCES

Abe Y, Ozaki Y, Kasuya J, Yamamoto K, Ando J, Sudo R, Ikeda M, Tanishita K. Endothelial progenitor cells promote directional three-dimensional endothelial network formation by secreting vascular endothelial growth factor. PloS one 2013; 8:e82085. [PubMed: 24312630]

Ai-Aql ZS, Alagl AS, Graves DT, Gerstenfeld LC, Einhorn TA. Molecular mechanisms controlling bone formation during fracture healing and distraction osteogenesis. J Dent Res 2008; 87:107–18. [PubMed: 18218835]

Akeson AL, Greenberg JM, Cameron JE, Thompson FY, Brooks SK, Wiginton D, Whitsett JA. Temporal and spatial regulation of VEGF-A controls vascular patterning in the embryonic lung. Dev Biol 2003; 264:443–55. [PubMed: 14651929]

Awada HK, Johnson NR, Wang YD. Sequential delivery of angiogenic growth factors improves revascularization and heart function after myocardial infarction. Journal of Controlled Release 2015; 207:7–17. [PubMed: 25836592]

Barnabe-Heider M, Di Marco M, Doane P, Genest MH, Gornea R, Guenette R, Leroy C, Lessard L, Martin JP, Wichoski U, Zacek V, Clark K, Krauss CB, Noble AJ, Behnke E, Feighery W, Levine I, Muthusi C, Kanagalingam S, Noulty R. Response of superheated droplet detectors of the PICASSO dark matter search experiment. Nuclear Instruments & Methods in Physics Research Section a-Accelerators Spectrometers Detectors and Associated Equipment 2005; 555:184–204.

Basmanav FB, Kose GT, Hasirci V. Sequential growth factor delivery from complexed microspheres for bone tissue engineering. Biomaterials 2008; 29:4195–204. [PubMed: 18691753]

Cai SS, Liu YC, Shu XZ, Prestwich GD. Injectable glycosaminoglycan hydrogels for controlled release of human basic fibroblast growth factor. Biomaterials 2005; 26:6054–67. [PubMed: 15958243]

Cao RH, Brakenhielm E, Pawliuk R, Wariaro D, Post MJ, Wahlberg E, Leboulch P, Cao YH. Angiogenic synergism, vascular stability and improvement of hind-limb ischemia by a combination of PDGF-BB and FGF-2. Nat Med 2003; 9:604–13. [PubMed: 12669032]

Carmeliet P, Jain RK. Molecular mechanisms and clinical applications of angiogenesis. Nature 2011; 473:298–307. [PubMed: 21593862]

Ceccarelli J, Putnam AJ. Sculpting the blank slate: How fibrin's support of vascularization can inspire biomaterial design. Acta Biomaterialia 2014; 10:1515–23. [PubMed: 23933102]

Fabiilli ML, Haworth KJ, Fakhri NH, Kripfgans OD, Carson PL, Fowlkes JB. The role of inertial cavitation in acoustic droplet vaporization. IEEE Trans Ultrason Ferroelectr Freq Control 2009; 56:1006–17. [PubMed: 19473917]

Fabiilli ML, Haworth KJ, Fakhri NH, Kripfgans OD, Carson PL, Fowlkes JB. The Role of Inertial Cavitation in Acoustic Droplet Vaporization. IEEE Transactions on Ultrasonics, Ferroelectrics, and Frequency Control 2009; 56:1006–17.

Fabiilli ML, Wilson CG, Padilla F, Martin-Saavedra FM, Fowlkes JB, Franceschi RT. Acoustic droplet-hydrogel composites for spatial and temporal control of growth factor delivery and scaffold stiffness. Acta Biomaterialia 2013.

Garvin KA, Hocking DC, Dalecki D. Controlling the Spatial Organization of Cells and Extracellular Matrix Proteins in Engineered Tissues Using Ultrasound Standing Wave Fields. Ultrasound in Medicine and Biology 2010; 36:1919–32. [PubMed: 20870341]

Jeon O, Kang SW, Lim HW, Choi D, Kim DI, Lee SH, Chung JH, Kim BS. Synergistic effect of sustained delivery of basic fibroblast growth factor and bone marrow mononuclear cell transplantation on angiogenesis in mouse ischemic limbs. Biomaterials 2006; 27:1617–25. [PubMed: 16174524]

Jeon O, Ryu SH, Chung JH, Kim BS. Control of basic fibroblast growth factor release from fibrin gel with heparin and concentrations of fibrinogen and thrombin. Journal of Controlled Release 2005; 105:249–59. [PubMed: 16088988]

Kawabata K-I, Sugita N, Yoshikawa H, Azuma T, Umemura S-I. Nanoparticles with Multiple Perfluorocarbons for Controllable Ultrasonically Induced Phase Shifting. Japanese Journal of Applied Physics 2005; 44:4548–52.

Kempen DHR, Lu LC, Heijink A, Hefferan TE, Creemers LB, Maran A, Yaszemski MJ, Dhert WJA. Effect of local sequential VEGF and BMP-2 delivery on ectopic and orthotopic bone regeneration. Biomaterials 2009; 30:2816–25. [PubMed: 19232714]

Kim S, Kang YQ, Krueger CA, Sen ML, Holcomb JB, Chen D, Wenke JC, Yang YZ. Sequential delivery of BMP-2 and IGF-1 using a chitosan gel with gelatin microspheres enhances early osteoblastic differentiation. Acta Biomaterialia 2012; 8:1768–77. [PubMed: 22293583]

Kripfgans OD, Fowlkes JB, Miller DL, Eldevik OP, Carson PL. Acoustic droplet vaporization for therapeutic and diagnostic applications. Ultrasound in Medicine and Biology 2000; 26:1177–89. [PubMed: 11053753]

Layman H, Li XY, Nagar E, Vial X, Pham SM, Andreopoulos FM. Enhanced Angiogenic Efficacy through Controlled and Sustained Delivery of FGF-2 and G-CSF from Fibrin Hydrogels Containing Ionic-Albumin Microspheres. Journal of Biomaterials Science-Polymer Edition 2012; 23:185–206. [PubMed: 21192837]

Lee HJ, Koh WG. Hydrogel Micropattern-Incorporated Fibrous Scaffolds Capable of Sequential Growth Factor Delivery for Enhanced Osteogenesis of hMSCs. Acs Appl Mater Inter 2014; 6:9338–48.

Lee KY, Mooney DJ. Hydrogels for tissue engineering. Chemical Reviews 2001; 101:1869–79. [PubMed: 11710233]

Li J, Wei YQ, Liu K, Yuan C, Tang YJ, Quan QL, Chen P, Wang W, Hu HZ, Yang L. Synergistic effects of FGF-2 and PDGF-BB on angiogenesis and muscle regeneration in rabbit hindlimb ischemia model. Microvasc Res 2010; 80:10–17. [PubMed: 20045007]

Marchioni C, Riccardi E, Spinelli S, dell'Unto F, Grimaldi P, Bedini A, Giliberti C, Giuliani L, Palomba R, Castellano AC. Structural changes induced in proteins by therapeutic ultrasounds. Ultrasonics 2009; 49:569–76. [PubMed: 19278707]

Markert CD, Guo XY, Skardal A, Wang Z, Bharadwaj S, Zhang YY, Bonin K, Guthold M. Characterizing the micro-scale elastic modulus of hydrogels for use in regenerative medicine. Journal of the Mechanical Behavior of Biomedical Materials 2013; 27:115–27. [PubMed: 23916408]

Martino MM, Briquez PS, Ranga A, Lutolf MP, Hubbell JA. Heparin-binding domain of fibrin(ogen) binds growth factors and promotes tissue repair when incorporated within a synthetic matrix. Proceedings of the National Academy of Sciences of the United States of America 2013; 110:4563–68. [PubMed: 23487783]

Miles CJ, Doering CR, Kripfgans OD. Nucleation pressure threshold in acoustic droplet vaporization. Journal of Applied Physics 2016; 120.

Moncion A, Arlotta KJ, Kripfgans OD, Fowlkes JB, Carson PL, Putnam AJ, Franceschi RT, Fabiilli ML. Design and Characterization of Fibrin-Based Acoustically Responsive Scaffolds for Tissue Engineering Applications. Ultrasound in Medicine and Biology 2016; 42:257–71. [PubMed: 26526782]

Moncion A, Arlotta KJ, O'Neill EG, Lin M, Mohr LA, Franceschi RT, Kripfgans OD, Putnam AJ, Fabiilli ML. In vitro and in vivo assessment of controlled release and degradation of acoustically-responsive scaffolds. Acta Biomaterialia 2016; 46:221–33. [PubMed: 27686040]

Moncion A, Arlotta KJ, O'Neill EG, Lin M, Mohr LA, Franceschi RT, Kripfgans OD, Putnam AJ, Fabiilli ML. In vitro and in vivo assessment of controlled release and degradation of acoustically responsive scaffolds. Acta Biomaterialia 2016; 46:221–33. [PubMed: 27686040]

Moncion A, Lin M, O'Neill EG, Franceschi RT, Kripfgans OD, Putnam AJ, Fabiilli ML. Controlled release of basic fibroblast growth factor for angiogenesis using acoustically-responsive scaffolds. Biomaterials 2017; 140:26–36. [PubMed: 28624705]

Mountford PA, Borden MA. On the thermodynamics and kinetics of superheated fluorocarbon phase-change agents. Advances in Colloid and Interface Science 2016; 237:15–27. [PubMed: 27574721]

Mountford PA, Smith WS, Borden MA. Fluorocarbon Nanodrops as Acoustic Temperature Probes. Langmuir 2015; 31:10656–63. [PubMed: 26359919]

Nehls V, Herrmann R, Huhnken M. Guided migration as a novel mechanism of capillary network remodeling is regulated by basic fibroblast growth factor. Histochemistry and Cell Biology 1998; 109:319–29. [PubMed: 9562381]

Rapoport N, Nam KH, Gupta R, Gao Z, Mohan P, Payne A, Todd N, Liu X, Kim T, Shea J, Scaife C, Parker DL, Jeong EK, Kennedy AM. Ultrasound-mediated tumor imaging and nanotherapy using drug loaded, block copolymer stabilized perfluorocarbon nanoemulsions. Journal of controlled release : official journal of the Controlled Release Society 2011; 153:4–15. [PubMed: 21277919]

Rapoport NY, Kennedy AM, Shea JE, Scaife CL, Nam K-H. Controlled and targeted tumor chemotherapy by ultrasound-activated nanoemulsions/microbubbles. Journal of Controlled Release 2009; 138:268–76. [PubMed: 19477208]

Reznik N, Shpak O, Gelderblom EC, Williams R, de Jong N, Versluis M, Burns PN. The efficiency and stability of bubble formation by acoustic vaporization of submicron perfluorocarbon droplets. Ultrasonics 2013; 53:1368–76. [PubMed: 23652262]

Reznik N, Williams R, Burns PN. Investigation of Vaporized Submicron Perfluorocarbon Droplets as an Ultrasound Contrast Agent. Ultrasound in Medicine and Biology 2011; 37:1271–79. [PubMed: 21723449]

Richardson TP, Peters MC, Ennett AB, Mooney DJ. Polymeric system for dual growth factor delivery. Nat Biotechnol 2001; 19:1029–34. [PubMed: 11689847]

Riess JG. Oxygen Carriers ("Blood Substitutes") - Raison d'Etre, Chemistry, and Some Physiology. Chemical Reviews 2001; 101:2797–919. [PubMed: 11749396]

Ruhrberg C, Gerhardt H, Golding M, Watson R, Ioannidou S, Fujisawa H, Betsholtz C, Shima DT. Spatially restricted patterning cues provided by heparin-binding VEGF-A control blood vessel branching morphogenesis. Genes & development 2002; 16:2684–98. [PubMed: 12381667]

Sahni A, Odrljin T, Francis CW. Binding of basic fibroblast growth factor to fibrinogen and fibrin. J Biol Chem 1998; 273:7554–59. [PubMed: 9516457]

Saik JE, Gould DJ, Watkins EM, Dickinson ME, West JL. Covalently immobilized platelet-derived growth factor-BB promotes antiogenesis in biomirnetic poly(ethylene glycol) hydrogels. Acta Biomaterialia 2011; 7:133–43. [PubMed: 20801242]

Schad KC, Hynynen K. In vitro characterization of perfluorocarbon droplets for focused ultrasound therapy. Physics in Medicine and Biology 2010; 55:4933–47. [PubMed: 20693614]

Sheeran PS, Luois SH, Mullin LB, Matsunaga TO, Dayton PA. Design of ultrasonically-activatable nanoparticles using low boiling point perfluorocarbons. Biomaterials 2012; 33:3262–9. [PubMed: 22289265]

Sheeran PS, Wong VP, Luois S, McFarland RJ, Ross WD, Feingold S, Matsunaga TO, Dayton PA. Decafluorobutane as a Phase-Change Contrast Agent for Low-Energy Extravascular Ultrasonic Imaging. Ultrasound in Medicine and Biology 2011; 37:1518–30. [PubMed: 21775049]

Tabata Y, Hijikata S, Muniruzzaman M, Ikada Y. Neovascularization effect of biodegradable gelatin microspheres incorporating basic fibroblast growth factor. Journal of Biomaterials Science-Polymer Edition 1999; 10:79–94. [PubMed: 10091924]

Tengood JE, Ridenour R, Brodsky R, Russell AJ, Little SR. Sequential Delivery of Basic Fibroblast Growth Factor and Platelet-Derived Growth Factor for Angiogenesis. Tissue Eng Pt A 2011; 17:1181–89.

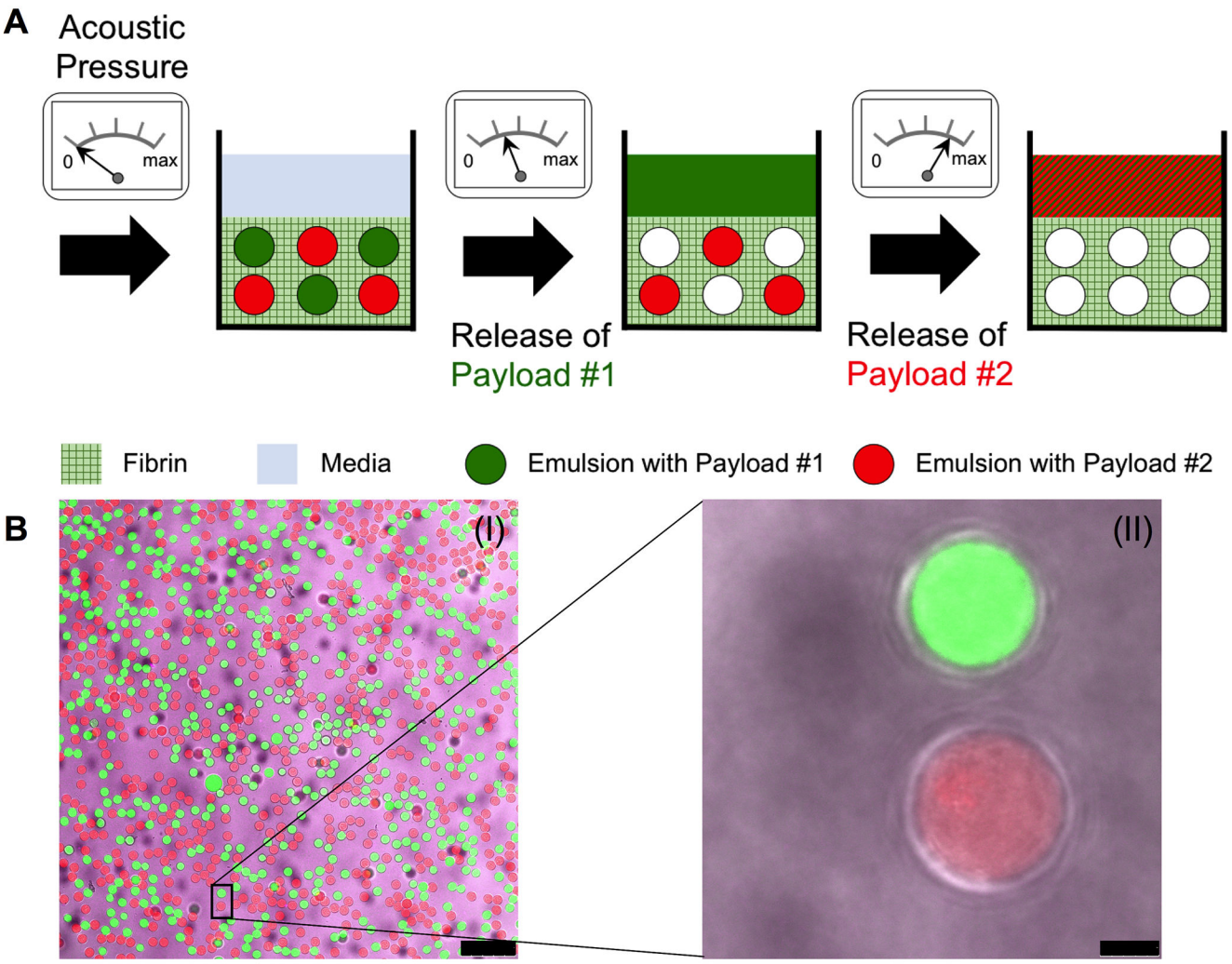

Figure 1:

(A) Sequential release of two payloads using an ARS. Two similarly-sized emulsions, each containing a different PFC and payload, are incorporated into an ARS. For release of payload #1, the ARS is exposed to US at an acoustic pressure above the ADV threshold of the emulsion with payload #1, but below the threshold of the emulsion containing payload #2. At a later time point, the same ARS is exposed to US at an acoustic pressure above the ADV threshold of the emulsion with payload #2, thus releasing payload #2. (B) Confocal microscopy images of an ARS with two payloads at 25× (I) and 100× (II) magnification. The ARS contained 0.67% (v/v) PFH emulsion with AF488-labelled dextran in the W_1 phase (green), 0.33% (v/v) PFHep emulsion with AF594-labelled dextran in the W_1 phase (red), and AF647-labelled fibrinogen (magenta) in the fibrin matrix. Scale bar equals 75 μm and 5 μm for B(I) and B(II), respectively.

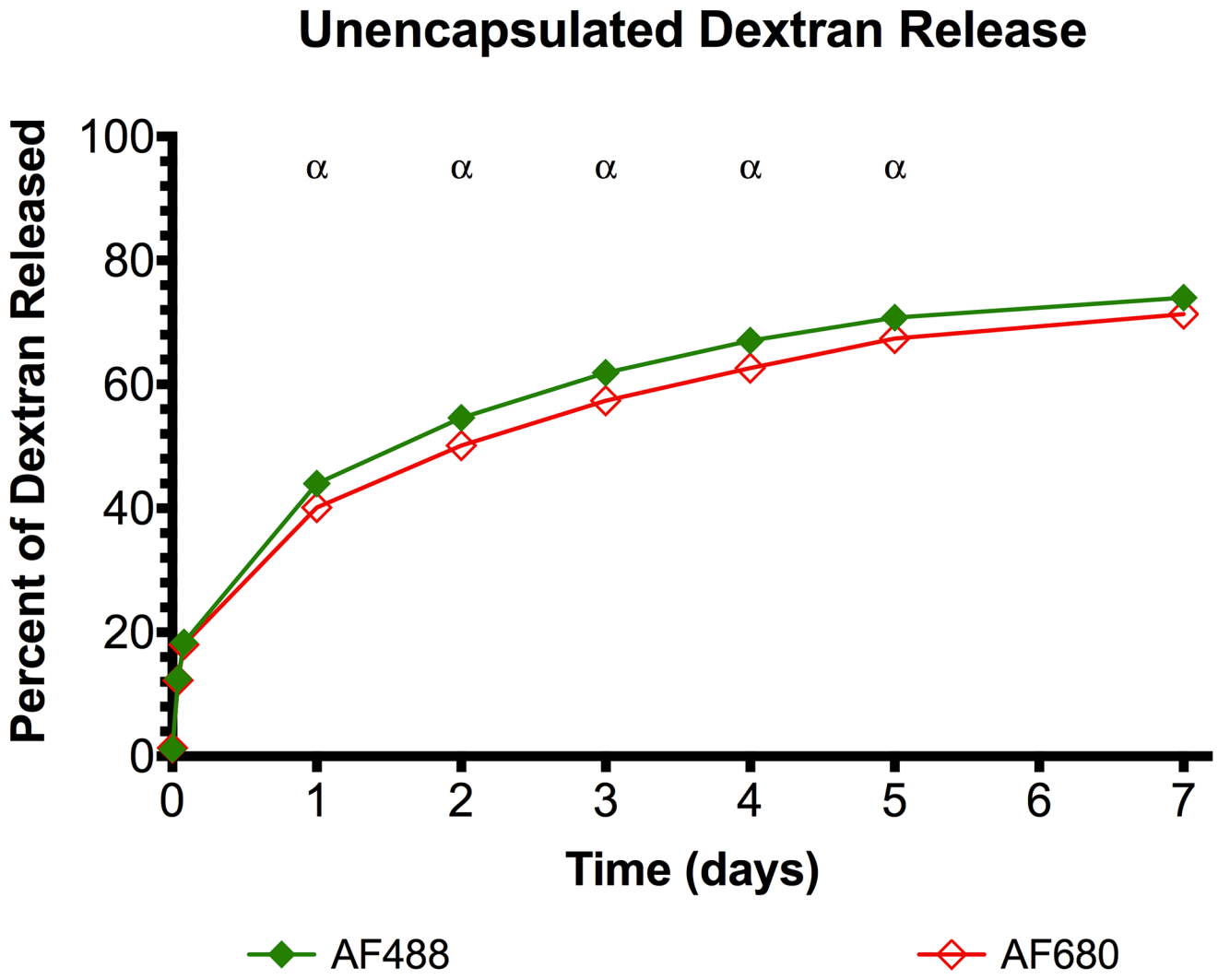

Figure 2:

Dextrans, incorporated directly into a conventional fibrin scaffold without any encapsulation, are released quickly. Statistically significant differences ($p < 0.05$) between AF488 and AF594 dextrans are denoted by α for n=5 samples.

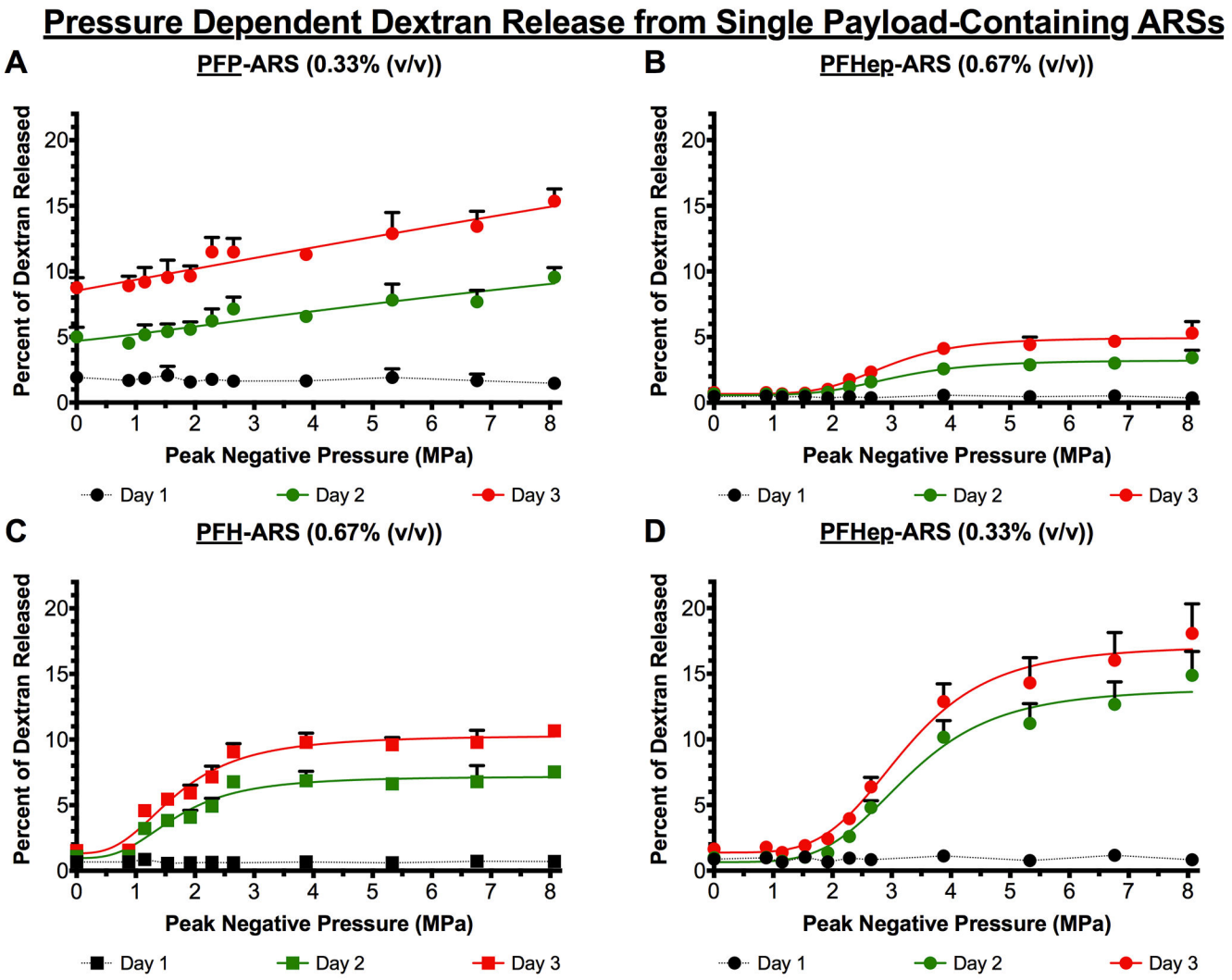

Figure 3:

The release of dextran was longitudinally measured as a function of acoustic pressure from ARSs containing (A) 0.33% (v/v) PFP emulsion (B) 0.67% (v/v) PFHep emulsion (C) 0.67% (v/v) PFH emulsion, and (D) 0.33% (v/v) PFHep emulsion. PFP and PFH emulsions contained AF488 dextran while PFHep emulsion contained AF594 dextran. In all cases, the dextran was incorporated into the W_1 phase of the emulsion and US exposure occurred one day after polymerization of the ARS. Statistics are based on n=5 measurements per condition. Curve fits are based on a 4-parameter sigmoidal model.

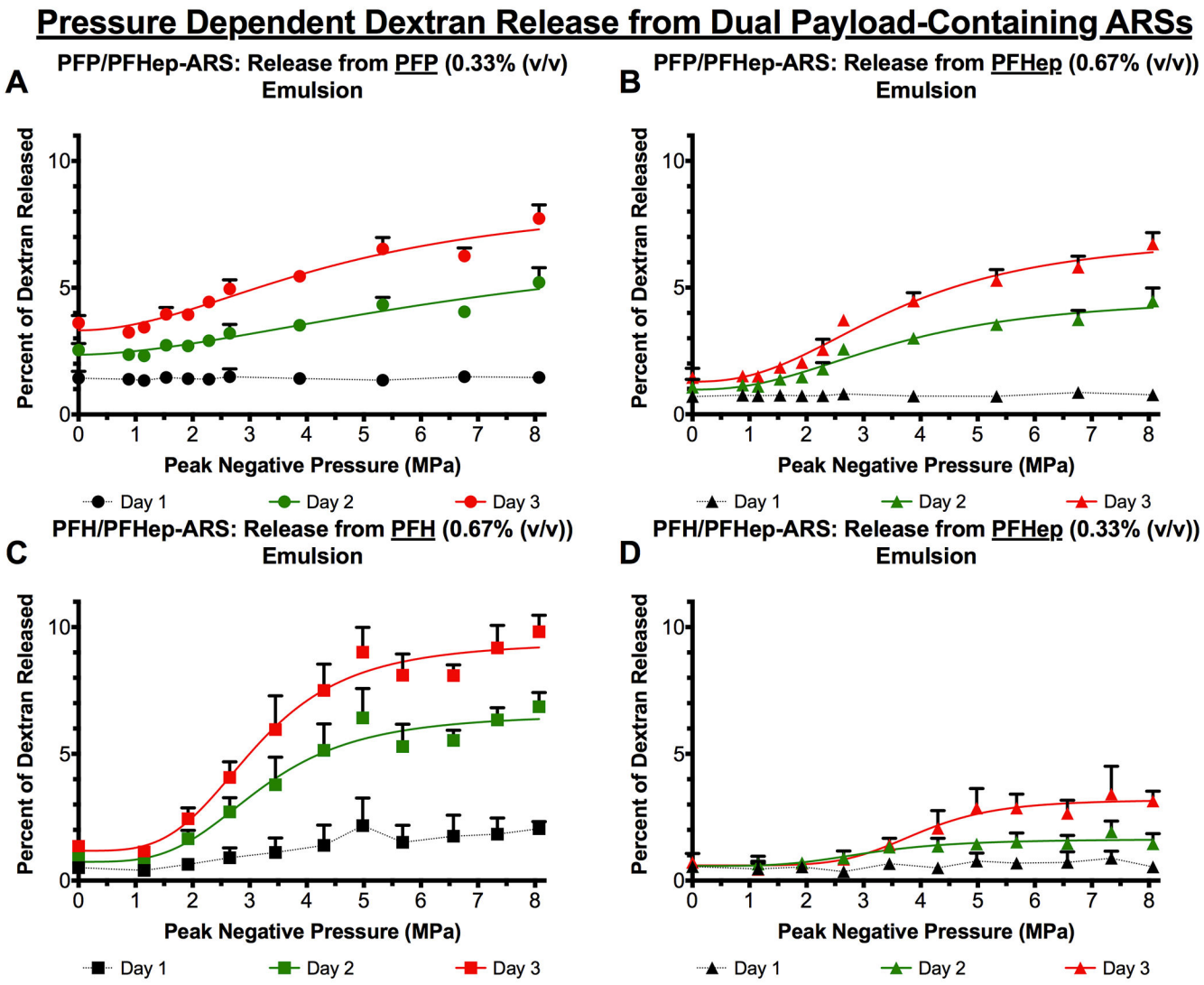

Figure 4:

The release of dextran was longitudinally measured as a function of acoustic pressure for dual payload ARSs. The release profiles from (A) 0.33% (v/v) PFP emulsion and (B) 0.67% (v/v) PFHep emulsion within PFP/PFHep-ARSs are shown. The release profiles from (C) 0.67% (v/v) PFH emulsion and (D) 0.33% (v/v) PFHep emulsion within PFH/PFHep-ARSs are shown. PFP and PFH emulsions contained AF488 dextran while PFHep emulsion contained AF594 dextran. Statistics are based on n=5 measurements per condition. Curve fits are based on a 4-parameter sigmoidal model.

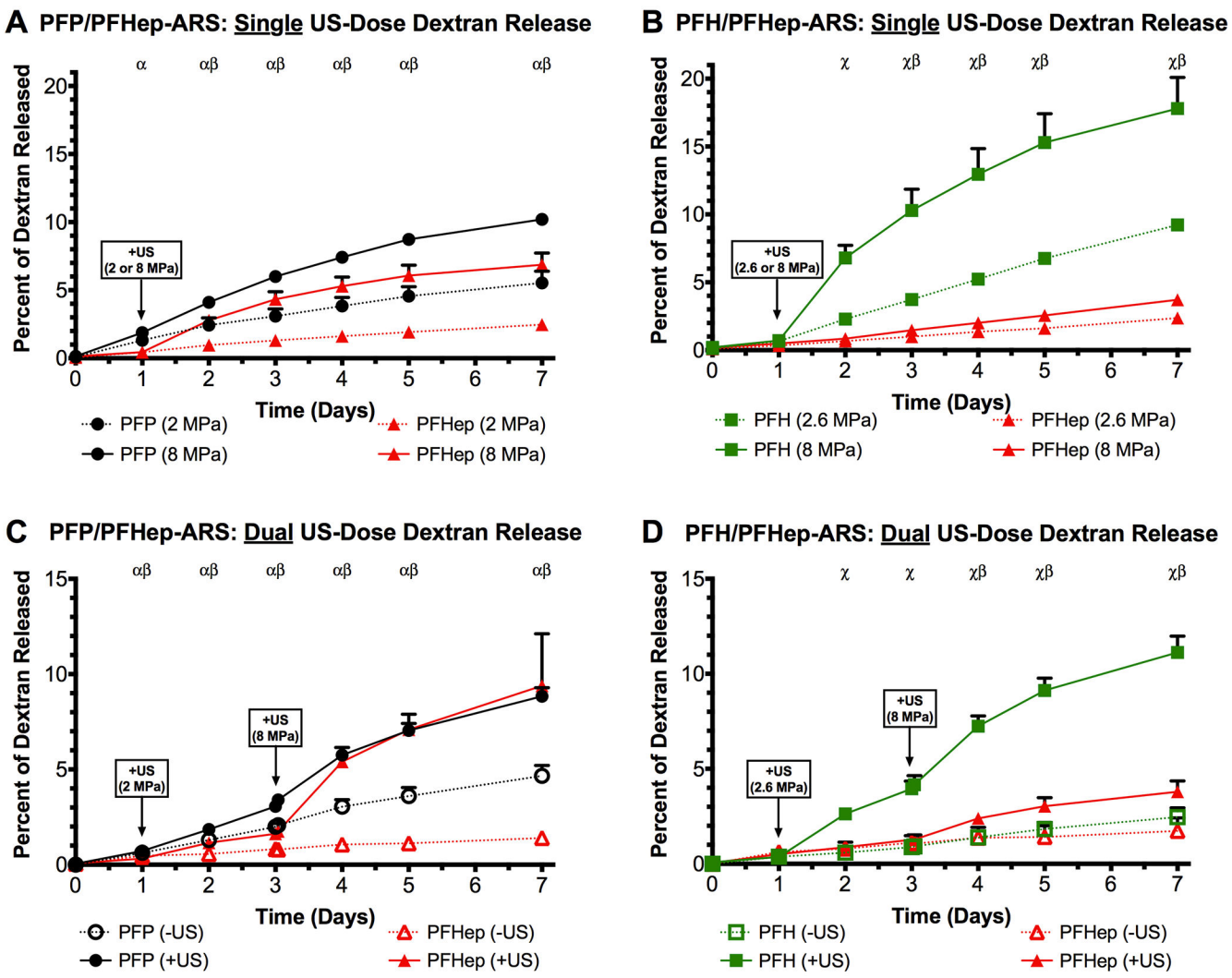

Figure 5:

Release profiles of (A) PFP/PFHep-ARSs and (B) PFH/PFHep-ARSs are shown following a single US exposure on day 1. For PFP/PFHep-ARSs, exposure was either at 2 or 8 MPa while for PFH/PFHep-ARSs, exposure was at 2.6 or 8 MPa. The release profiles for PFP/PFHep-ARSs and PFH/PFHep-ARSs following sequential US exposures on day 1 and day 3 are shown in (C) and (D), respectively. PFP/PFHep-ARSs were exposed to 2 MPa (day 1) and 8 MPa (day 3). PFH/PFHep-ARSs were exposed to 2.6 MPa (day 1) and 8 MPa (day 3). PFP and PFH emulsions contained AF488 dextran while PFHep emulsion contained AF594 dextran. Statistically significant differences ($p < 0.05$) between AF488 and AF594 are denoted by α: PFP (+US vs. −US), χ: PFH (+US vs. −US), and β: PFHep (+US vs. −US) for n=5 samples.

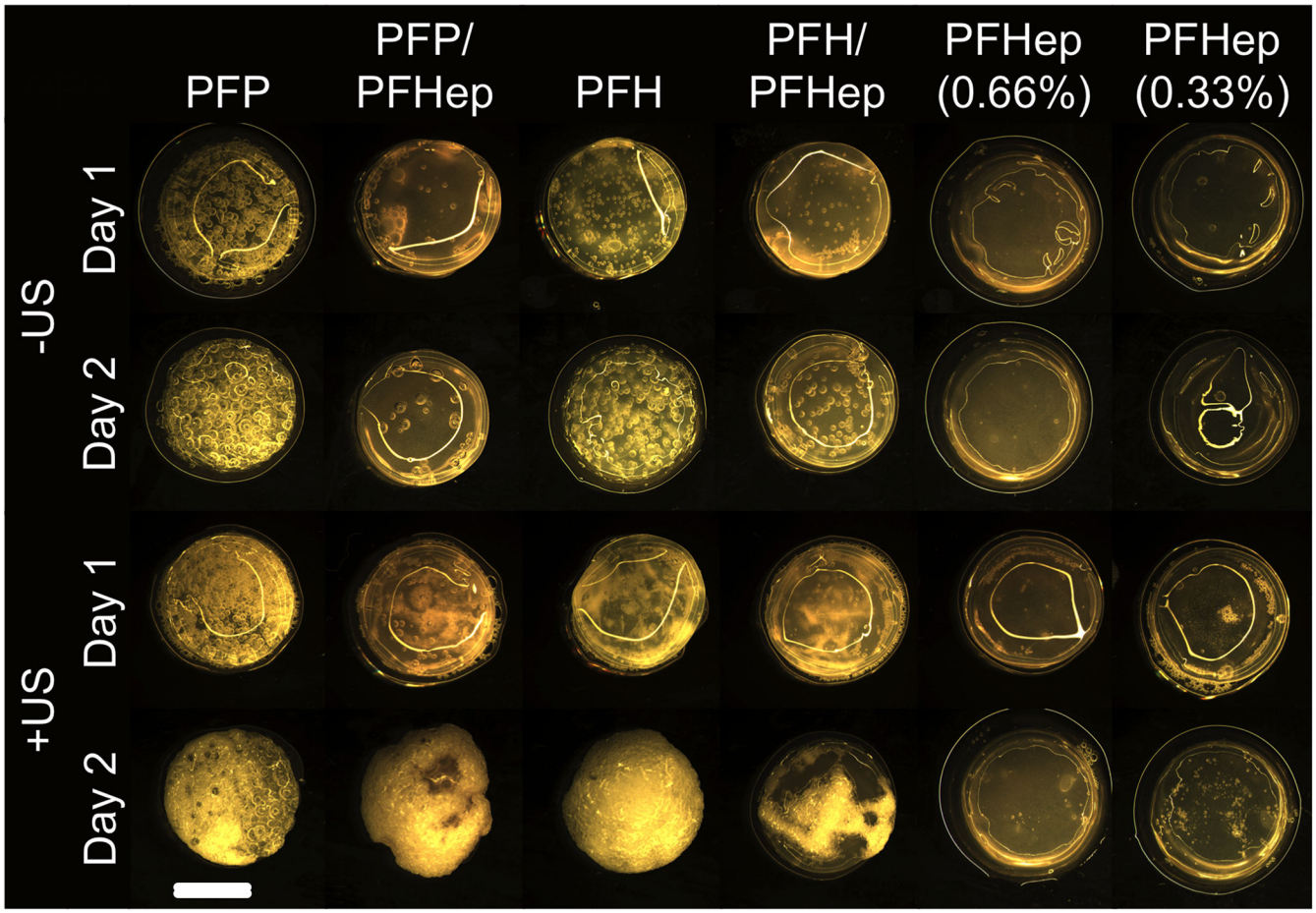

Figure 6:

Macroscopic images of different ARS formulations as a function of time and US exposure. ARSs with a higher boiling point PFC (e.g., PFHep-ARSs) showed less bubble formation than lower boiling point ARSs (e.g., PFP-ARSs). Applying US to generated ADV in the ARSs resulted in more bubble formation on day 2 relative to the comparable condition in the absence of US. With some ARSs, the reflection of light off of the top surface is evident. Scale bar equals 8 mm.

Table 1:

Physiochemical and acoustic characteristics of the double emulsions used in the ARSs. The ADV and IC thresholds are for ARSs with a single emulsion type.

PFC Composition	Emulsion 1			Emulsion 2			US Pressure (MPa)	Day of US Exposure
	PFC	Payload	Volume %	PFC	Payload	Volume %		
PFP	PFP	AF488	0.33	-	-	-	0-8	1
PFP/PFHep	PFP	AF488	0.33	PFHep	AF680	0.67	0-8	1
							2 or 8	1
							2 and 8	1 and 3
PFH	PFH	AF488	0.67	-	-	-	0-8	1
PFH/PFHep	PFH	AF488	0.67	PFHep	AF680	0.33	0-8	1
							2 or 8	1
							2 and 8	1 and 3
PFHep	PFHep	AF680	0.67	-	-	-	0-8	1
PFHep	PFHep	AF680	0.33	-	-	-	0-8	1

Ultrasound Med Biol. Author manuscript; available in PMC 2019 November 01.

Table 2:

List of all ARSs used in the presented experiments, as well as the ultrasound pressures interrogated and the days of exposure.

Perfluorocarbon in Emulsion	Boiling point (°C)	Encapsulation Efficiency (%)	Mean Diameter (μm)	Coefficient of Variance (%)	Concentration (#/mL)	ADV Threshold (MPa)	IC Threshold (MPa)
PFP (C_5F_{12})	**29**	95.90 ± 4.42	12.56 ± 0.65	5.08 ± 1.81	4.50E8 ± 1.41E8	1.42 ± 0.14	2.84 ± 1.45
PFH (C_6F_{14})	**56**	99.60 ± 0.51	12.92 ± 0.17	3.42 ± 0.65	4.02E8 ± 1.01E8	1.92 ± 0.37	3.77 ± 0.16
PFHep (C_7F_{16})	**84**	99.70 ± 0.23	13.09 ± 0.21	3.19 ± 0.20	4.29E8 ± 4.93E7	2.18 ± 0.37	4.10 ± 0.10